Supplementary Information for *Acta Phys. -Chim. Sin.* 2016, *32* (1), 349–355
doi: 10.3866/PKU.WHXB201512073

$Na_2Ti_3O_7$ 纳米片原位制备与钠离子电池负极材料应用

陈程成[1] 张 宁[1] 刘永畅[1] 王一菁[1] 陈 军[1,2,*]

([1]南开大学化学学院，先进能源材料教育部重点实验室，天津 300071；
[2]南开大学，天津化学化工协同创新中心，天津 300071)

In-situ Preparation of $Na_2Ti_3O_7$ Nanosheets as High-Performance Anodes for Sodium Ion Batteries

CHEN Cheng-Cheng[1] ZHANG Ning[1] LIU Yong-Chang[1] WANG Yi-Jing[1]

CHEN Jun[1,2,*]

([1]*Key Laboratory of Advanced Energy Materials Chemistry* (*Ministry of Education*), *College of Chemistry, Nankai University, Tianjin 300071, P. R. China*; [2]*Collaborative Innovation Center of Chemical Science and Engineering, Nankai University, Tianjin 300071, P. R. China*))

[*]Corresponding author. Email: chenabc@nankai.edu.cn; Tel: +86-22-23506808.

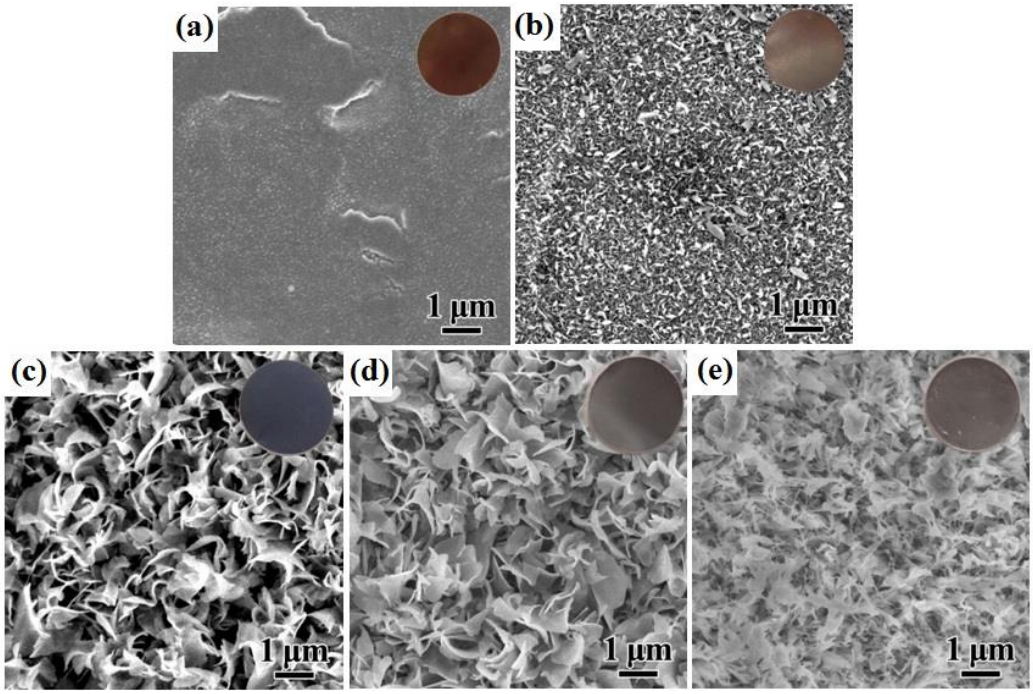

Fig.S1 SEM images of the NTO precursor in different concentrations of NaOH solution ((a) 0, (b) 0.1, (c) 0.5, (d) 1, (e) 2 mol·L^{-1}) and corresponding NTO/Ti wafers

Further discussion (concentration optimization)

In order to obtain the appropriate mass, uniform morphology, and well crystallinity $Na_2Ti_3O_7$ electrodes, the reaction concentration and temperature have been optimized. Fig.S1 shows the SEM images of precursors reacted in 0, 0.1, 0.5, 1, 2 mol·L^{-1} sodium hydroxide solution, respectively. It can be observed clearly that the corrosion degree gradually deepened with concentration increase. Fig.S1a exhibits that the surface of Ti foil is very smooth implying that Ti foil can not be corroded by neutral solution. At 0.1 mol·L^{-1} alkaline solution, slight corrosion reaction occurs on the surface. Fig.S1b displays numerous regular nanosize sheets grow on the surface of Ti foils. Whereas, if the concentration of sodium hydroxide solution above 0.5 mol·L^{-1}, the Ti surface suffered serious corrosion shown in Fig.S1c, d and e. It is worth noting that the Ti foils reacted in 0.5 and 1 mol·L^{-1} reveal interconnected nanosheets with uniform arrangement. But the nanosheets, bulks and nanowires mixed structure appears in 2

mol·L^{-1} alkaline solution implying the serious corrosion. Furthermore, from the insert images of visible Ti wafer, the color of Ti foil surface change from puce to light grey with concentration increase of sodium hydroxide solution. It indicates that the amount of $Na_2Ti_3O_7$ precursor is increase on the surface of Ti foils.

Table S1 The content of Na and Ti in 1 mol·L^{-1} NaOH solution before and after reaction by ICP measurement

Sample	Na (wt.%)	Ti (wt. %)
1 mol·L^{-1} (before reaction)	1.88	≤ 0.0001
1 mol·L^{-1} (after reaction)	1.80	≤ 0.0001

Table S2 The mass increment of Ti wafers (one sided) reacted in different concentration NaOH solution after calcined

Sample/(mol·L^{-1})	0	0.1	0.5	1	2
Mass increment/mg	< 0.05	< 0.05	0.2	0.3	0.5

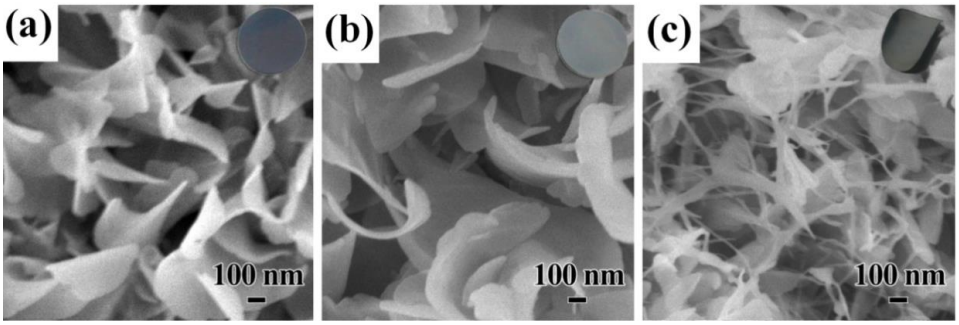

Fig.S2 SEM images of $Na_2Ti_3O_7$ calcined at 400 °C ((a) 0.5, (b) 1, (c) 2 mol·L^{-1}) and corresponding NTO/Ti wafers

Further discussion: To accurately determine the amount of generated $Na_2Ti_3O_7$, it is necessary to detect if any Ti dissolved in the solution leading to the mass loss of Ti

wafers. Through inductively coupled plasma (ICP) measurement (Table S1), Ti content has always kept below 1 ppm before and after reaction. It indicates that almost no measured Ti dissolve in the solution during the reaction. Thus, the increased weight could be reasonably attributed to Na and O (52.3 wt. % of $Na_2Ti_3O_7$). The mass increases of Ti wafer reacted in different concentration have been weighed, displaying in above Table S2. Therefore, the mass of active material can be calculated as follows: (prepared in 1 mol·L^{-1}, about 0.3 mg).

$$\frac{\text{increased weight} \div 52.3\ \%}{\text{area of current collector}} = \frac{0.3 \div 52.3\ \%}{0.5^2 \times 3.14} = 0.74\ \text{mg} \cdot \text{cm}^{-2}$$

The loading density of anode is about 0.74 mg cm^{-2}. Fig.S2 shows the SEM images of $Na_2Ti_3O_7$. All the samples keep the original morphology. However, from the insert images of Ti wafers, the Ti wafer reacted in 2 mol·L^{-1} solution was curly, which may be due to the relative serious corrosion destroying its mechanical properties. Therefore, according to morphology uniformity and the amount of active material, Ti wafers reacted in 1 mol·L^{-1} NaOH solution were considered to be the best candidate for electrode material.

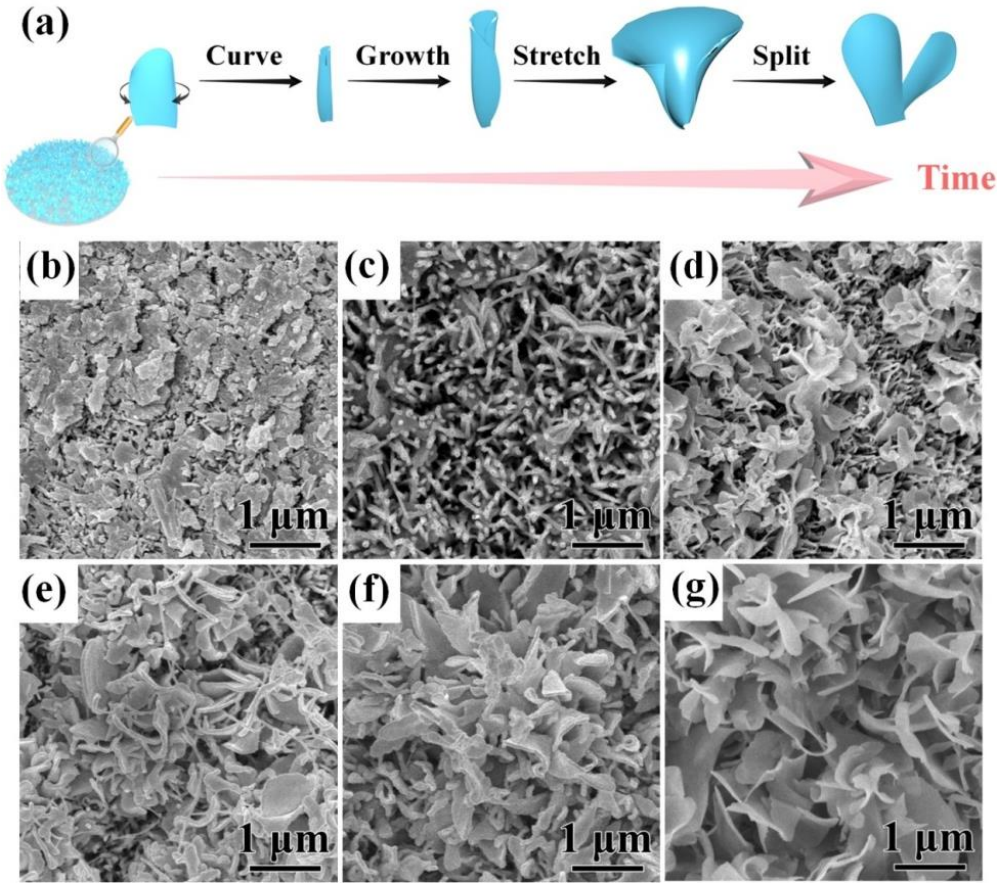

Fig.S3 (a) Schematic illustration of the probable growth process of $Na_2Ti_3O_7$ precursor during the corrosion reaction.SEM images of $Na_2Ti_3O_7$ precursors in 1 mol·L^{-1} NaOH solution with different reaction time of (b) 3, (c) 6, (d) 9, (e) 12, (f) 18 and (g) 24 h

Further discussion

The probable growth process of $Na_2Ti_3O_7$ waved nanosheets on Ti foil has been investigated through a series of time-dependent experiments. The schematic of morphology evolution is displayed in Fig.S3a. Precursors were collected at different reaction time (3, 6, 9, 12, 18, 24 h). The evolution of structure and morphologies were observed by scanning electron microscope (SEM). At the beginning of 3 h, the surface of Ti foil shows rough slices and particles due to the slight alkaline corrosion (Fig.S3b). As time extended to 6 h, the slices gradually roll into nanotubes with 60 nm in diameter owing to the bending stress. They uniformly distributed on the Ti surface

(Fig.S3c). In the next 3 h, the nanotubes may grow bigger, and then stretch forming curly nanosheets. The new generated nanosheets grow on the nanotubes due to the further corrosion shown in Fig.S3d. For the reaction time equal to 12 h, the interconnected nanosheets evolved to petal structure. Noting that interlaced nanotubes is still observed between the sheets (Fig.S3e). When the time reached 18 h, only waved nanosheets appear on the surface (Fig.S3f). Subsequently, when the time extends to 24 h, the nanosheets gradually become wider and thinner shown in Fig.S3g. The overall appearance would not change with the time increase except for the enhancement of thickness (Fig.S4). Thus, the morphology of NTO can be easily controlled through hydrothermal time.

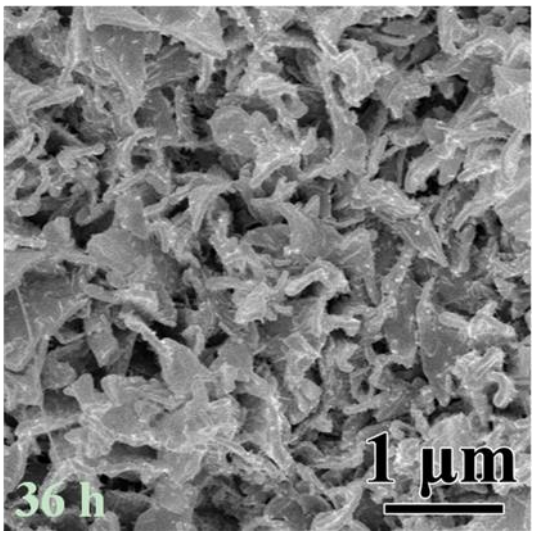

Fig.S4 SEM image of NTO precursor reacted for 36 h in 1 mol·L^{-1} NaOH solution

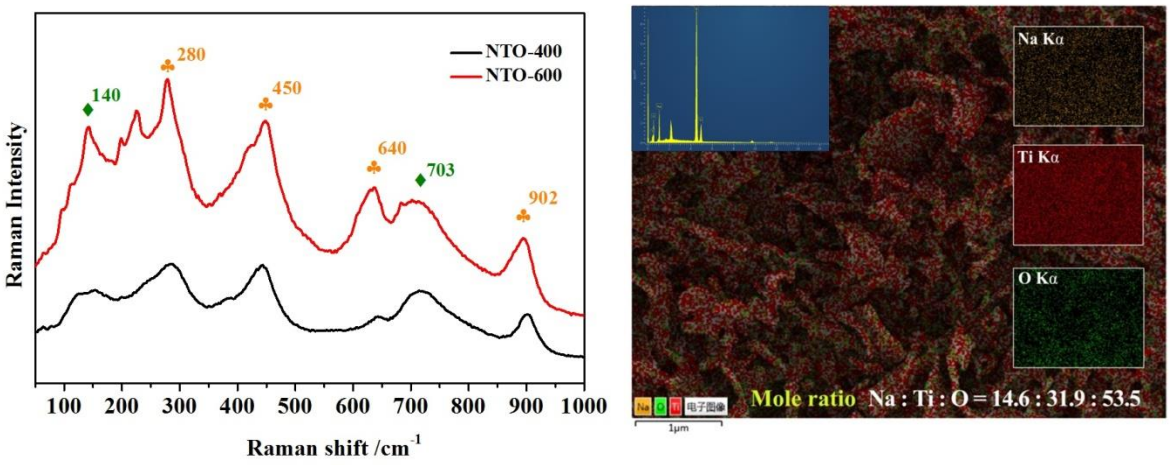

Fig.S5 (a) Raman spectrum of NTO-400 and NTO-600, (b) the SEM-EDX of NTO-600

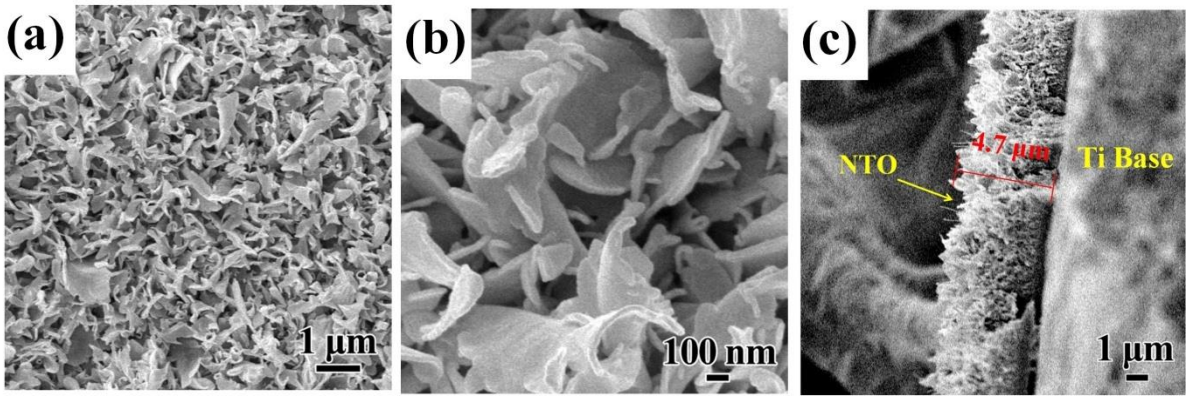

Fig.S6 SEM images including (a, b) front and (c) cross-sectional of NTO-400

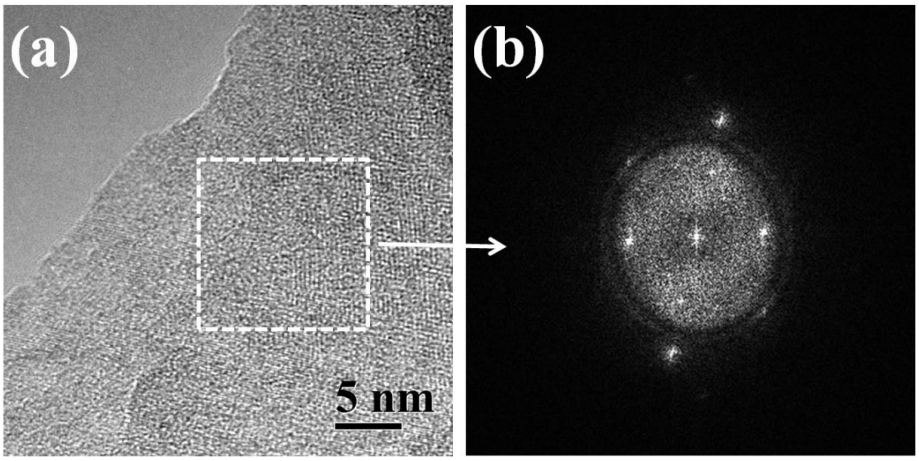

Fig.S7 TEM images of (a) NTO-400 and (b) corresponding Fourier transformation of selected areas

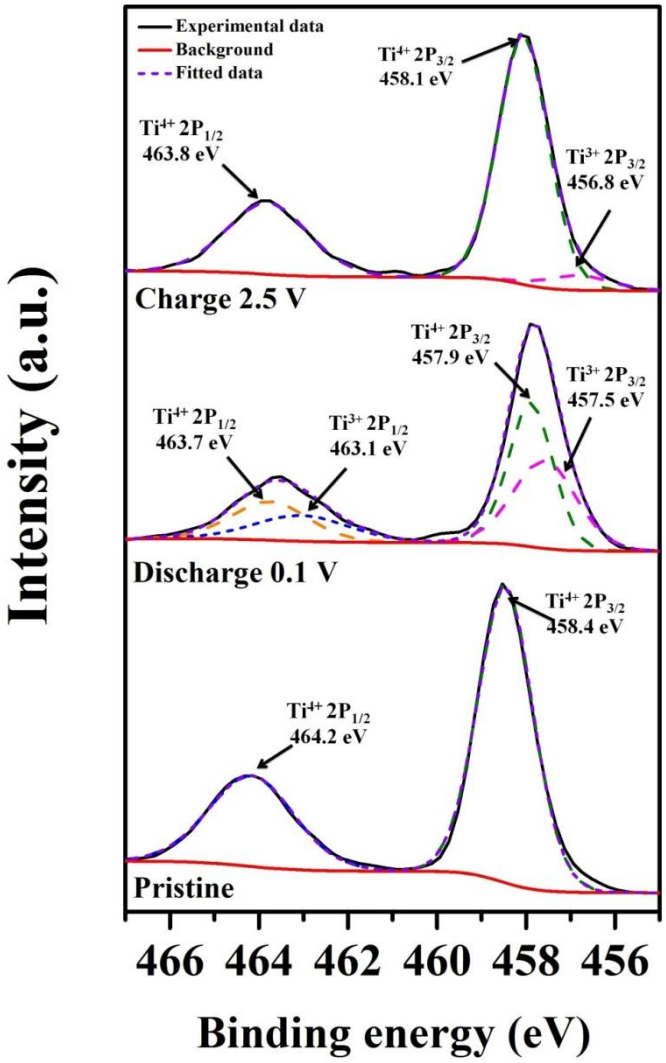

Fig.S8 XPS spectra of Ti in 1-600 NTO at different charge and discharge states

Further discussion: In order to further identify the valence evolution of NTO during the electrochemical reaction, XPS were employed at different charge and discharge states of Ti in NTO-600 electrode. As shown in Fig.S8, the pristine NTO-600 has two obvious peaks at 458.4 and 464.2 eV corresponding to Ti $2p_{3/2}$ and Ti $2p_{1/2}$ core level binding energies of Ti^{4+}, respectively. After discharging to 0.1 V, the whole peaks shift to the low binding energy (about 0.8 eV) and the half peak widths enlarge, implying the existence of Ti^{3+}. Large part of Ti^{3+} could be seen in the fitting curves. This process corresponds to the reduction reaction from Ti^{4+} to Ti^{3+}, when Na^{+} inserts into the cell structure. Whereas, after charging to 2.5 V, the whole peaks return to the high binding energy, which is attributed to the oxidation reaction from Ti^{3+} to Ti^{4+}.

However, it is worth noting that the peaks are not completely recovered. The slight shift about 0.3 eV indicates that some residual Ti^{3+} exist in the recharged NTO-600 electrode.

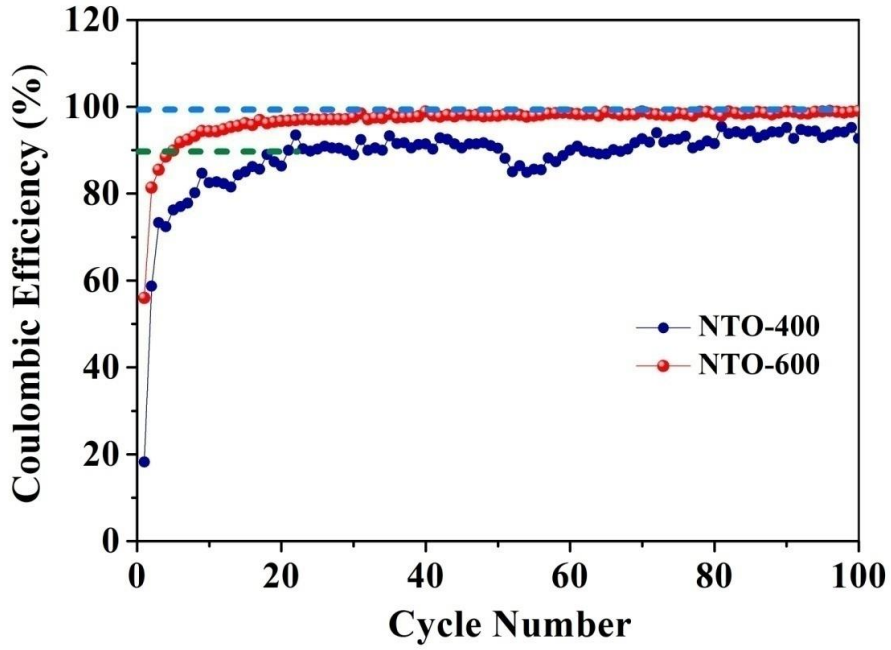

Fig.S9 Coulombic efficiency of NTO-400 and NTO-600 during the 100 cycles

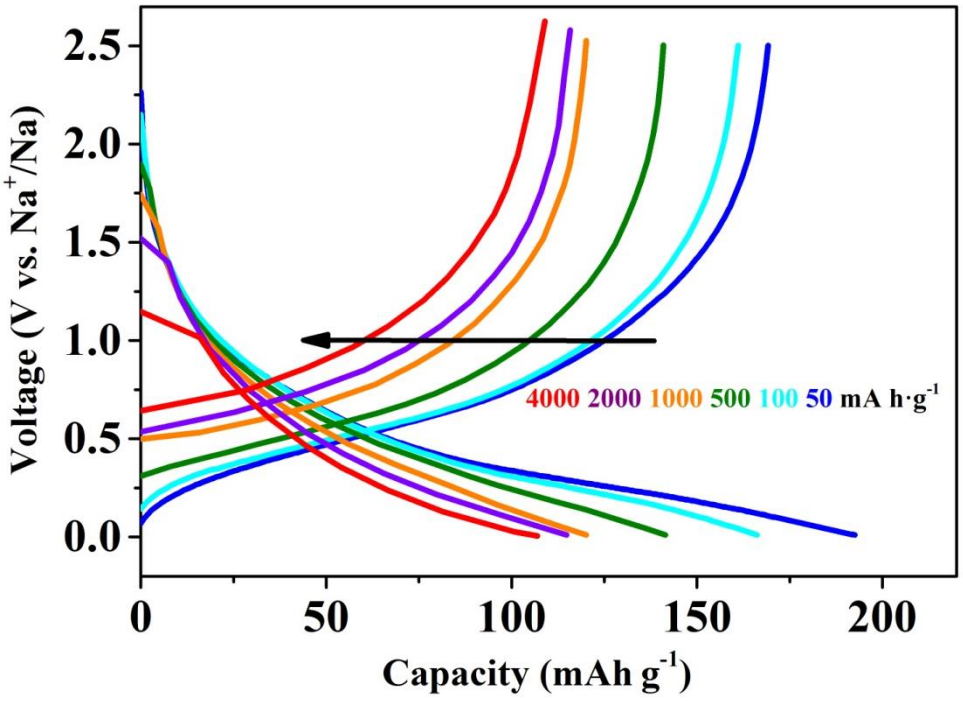

Fig.S10 Charge-discharge curves of NTO-600 at different rates

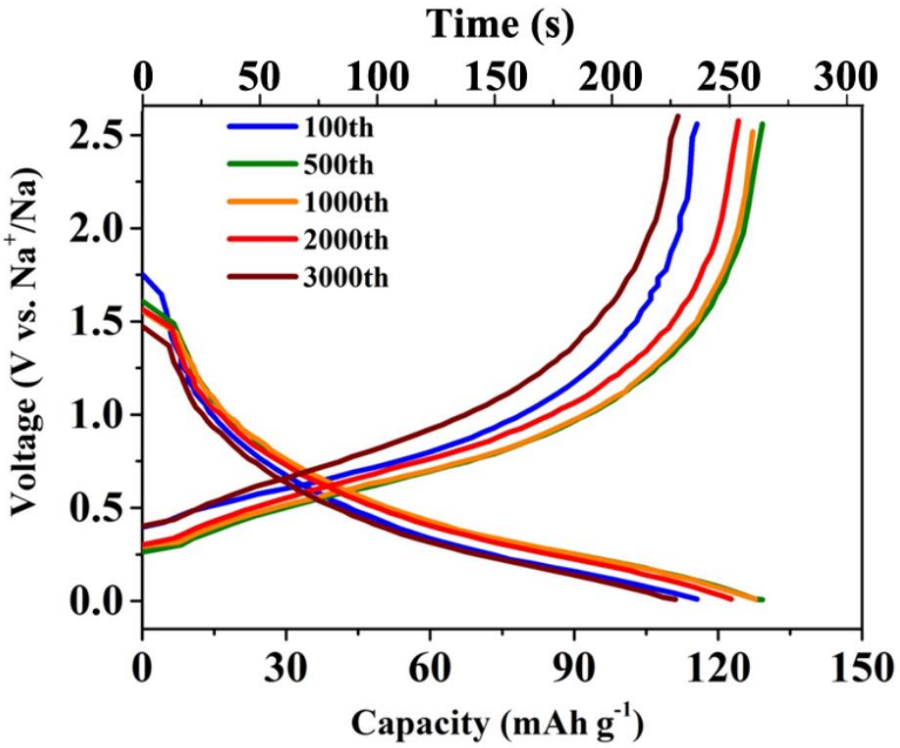

Fig.S11 Charge-discharge profiles of selected cycles during the 3000 cycles

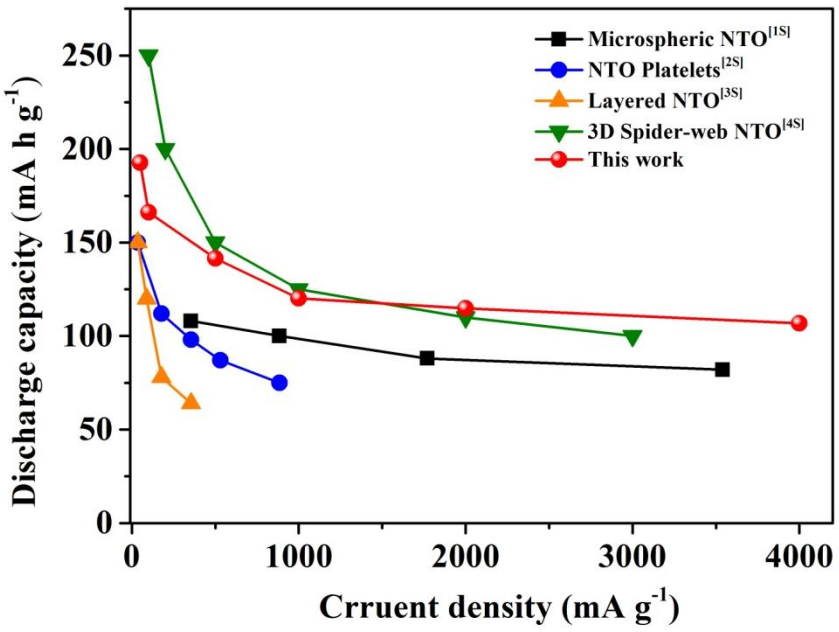

Fig.S12 Comparison of rate capability of NTO-600 electrode with other $Na_2Ti_3O_7$ based high rate electrodes reported recently

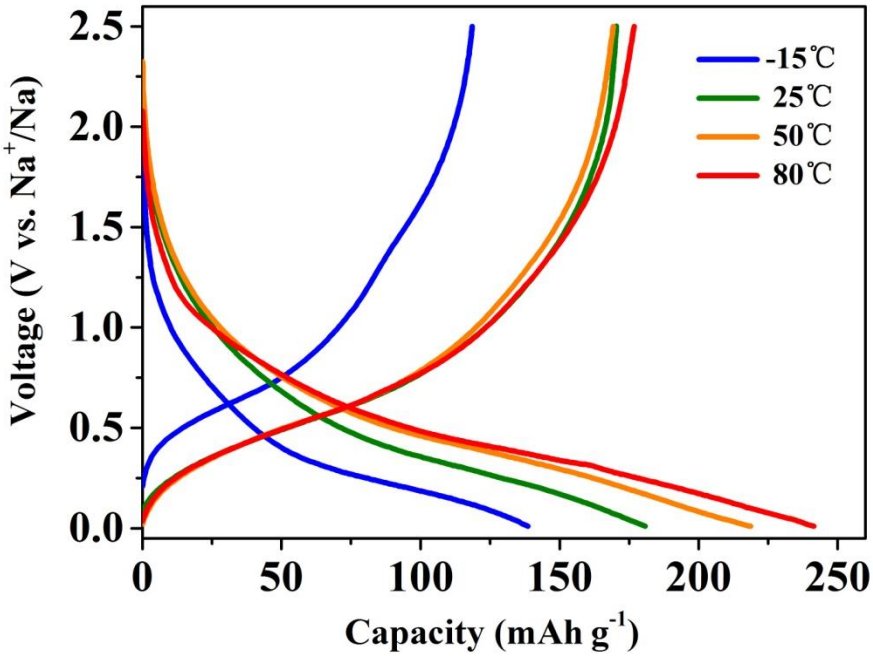

Fig.S13 Charge-discharge profilesof NTO-600 at 50 mA g^{-1}at different temperatre

GITT discussion

$$D_{\mathrm{GITT}} = \frac{4}{\pi}\left(\frac{m_{\mathrm{B}}V_{\mathrm{m}}}{M_{\mathrm{B}}S}\right)^2\left(\frac{\Delta E_{\mathrm{S}}}{\tau(\mathrm{d}E_{\tau}/\mathrm{d}\sqrt{\tau})}\right)^2 \quad \left(\tau \ll \frac{l^2}{D_{\mathrm{GITT}}}\right)$$ [S5]

where τ is the time period of the current pulse during the charge for a constant current value, m_{B} is the mass of the active material in electrode, M_{B} is molecular weight and V_{m} is its molar volume, S is the total contact area of electrode with electrolyte, E_{τ} is cell voltage, ΔE_{s} is the difference in the open circuitvoltage measured at the end of the relaxation period for two successive steps, l is the thickness of electrode. For the linear relationship between E_{τ} with $\tau_{1/2}$ shown in the insert image, the equation can be simplified as:

$$D_{\mathrm{GITT}} = \frac{4}{\pi\tau}\left(\frac{m_{\mathrm{B}}V_{\mathrm{m}}}{M_{\mathrm{B}}S}\right)^2\left(\frac{\Delta E_{\mathrm{S}}}{\Delta E_{\tau}}\right)^2 \qquad \left(\tau \ll \frac{l^2}{D_{\mathrm{GITT}}}\right)$$

Table S3 The diffusion coefficient of general material for sodium ion battery reported recently

Sample	$D_{Na+}/(cm^2 s^{-1})$
$Na_2Ti_3O_{7\ bulk}$[S2]	3.48×10^{-12}
$Na_{0.44}MnO_2$[S6]	9.15×10^{-12}
$Na_2V_6O_{16}$[S7]	2.46×10^{-14}
$Na_4Mn_9O_{18}$[S2]	$\sim 1\times10^{-15}$
Sb[S8]	5.1×10^{-13}
NaxGe[S9]	1.6×10^{-13}

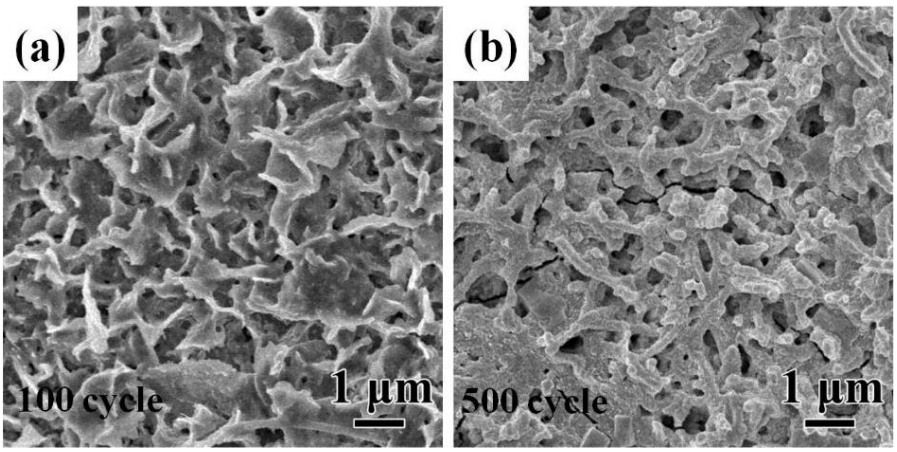

Fig.S14 SEM images of NTO-600 after (a) 100 cycles, and (b) 500 cycles at current density of 2000 mA g^{-1}

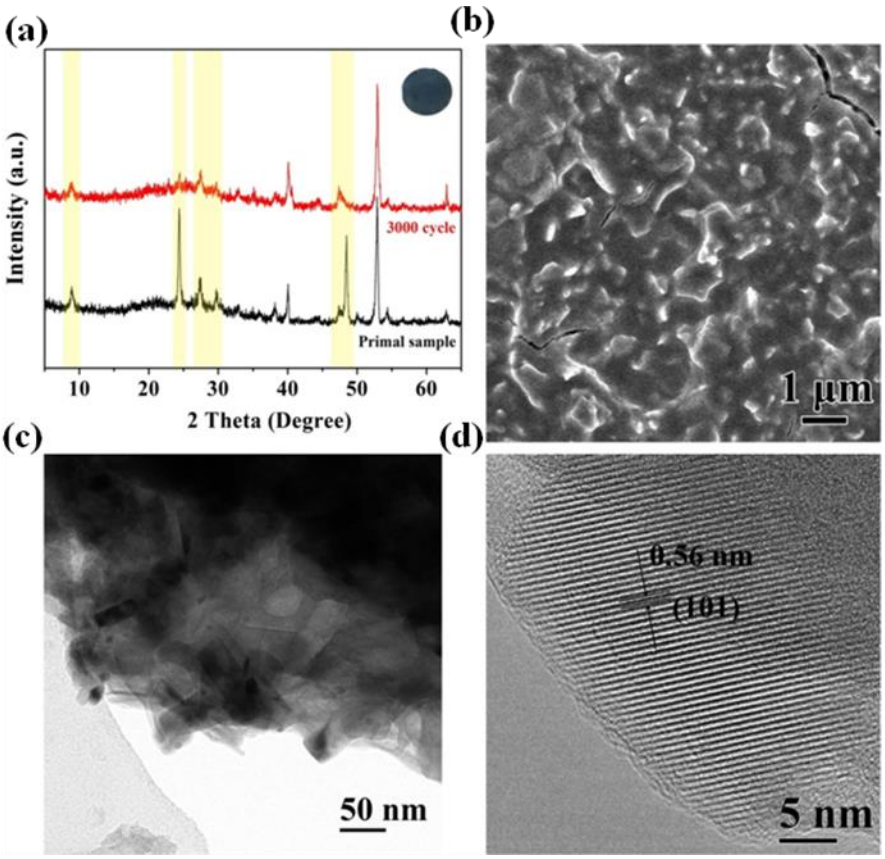

Fig.S15 (a) Comparison of XRD pattern of pristine NTO-600 with that after 3000 cycles, (b) SEM image of NTO-600 electrode after 3000 cycles, TEM images of NTO-600 after 3000 cycles at (c) low-resolution and (d) high-resolution

Further discussion

The structure and morphology characterizations of NTO-600 electrodes after 3000 cycles have been measured in Fig.S15. The XRD patterns (Fig.S15a) show that there are no new peaks appearing after 3000 cycles. It indicates that the intercalation-type reaction has no ruinous influence on the lattice structure. The Na^+ insert into the zigzag layers of $Na_2Ti_3O_7$ while the titanium octahedron cages construction is stable displayed in below eqn.

$$Na_2Ti_3O_7 + xNa^+ + xe^- \leftrightarrow Na_{2+x}Ti_3O_7 \ (0<x<3)$$

The insert image shows the accordant color of Ti wafer implying uniform distribution of active material after 3000 cycles. This verifies the strong adhesion of the binder-free electrode. Moreover, the SEM image of NTO-600 electrodes after 3000

cycles is shown in Fig.S15b. The irreversible substances adhere to the surface and the sheets agglomerate into chunk, which may result in the capacity loss. The corresponding TEM image (Fig.S15c) exhibits the cross nanosheets forming a bulk without any pulverization. The HR-TEM image (Fig.S15d) reveals that the nanosheets maintain obvious lattice fringes implying the well crystallinity after 3000 cycles.

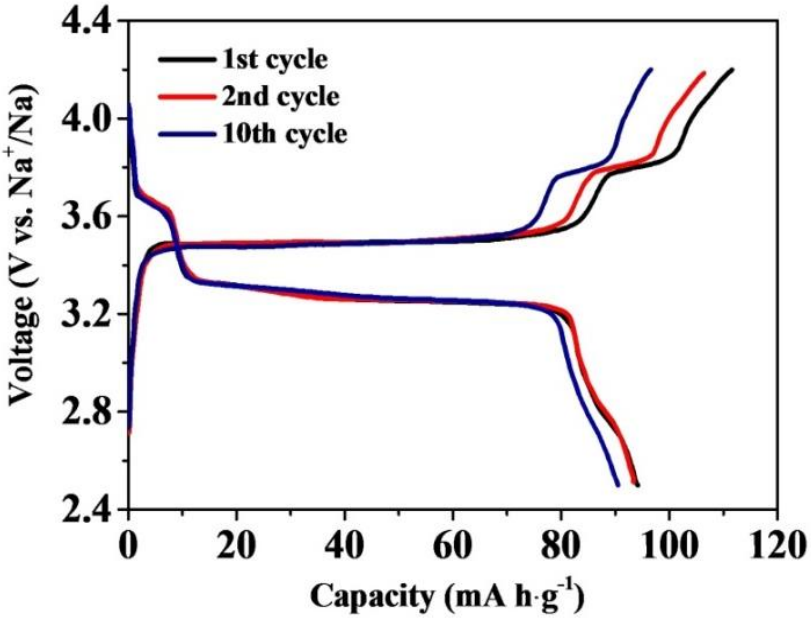

Fig.S16 Charge-discharge profiles of $NaVPO_4F$ at 50 mA g^{-1} of half-cell

The capacity balance of cathode and anode in full SIB.

The reversible capacity of anode (NTO) and cathode ($NaVPO_4F$) is about 175 and 90 mAh g^{-1}, respectively. The capacity of anode is excess 10 % to prevent the precipitation of Na. Thus, the mass ratio of anode and cathode is carefully calculated as 1:1.77 as follows:

$$\frac{\text{cathode mass}}{\text{anode mass}} = \frac{\text{anode capacity}}{\text{cathode capacity}} = \frac{175/1.1}{90} = 1.77$$

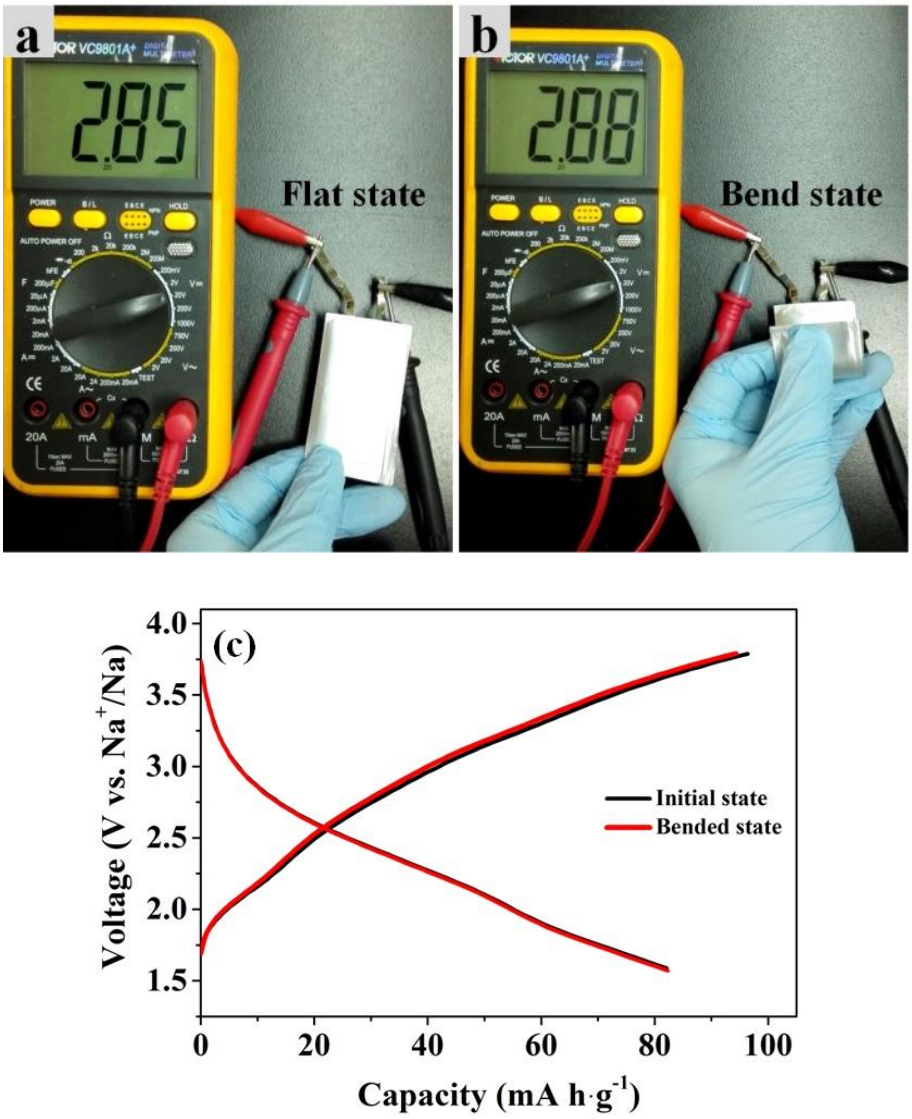

Fig.S17 Open circuit voltage of the (a) initial state and (b) bended state of the full SIB. (c) Working voltage of the initial state and bended state of the full SIB

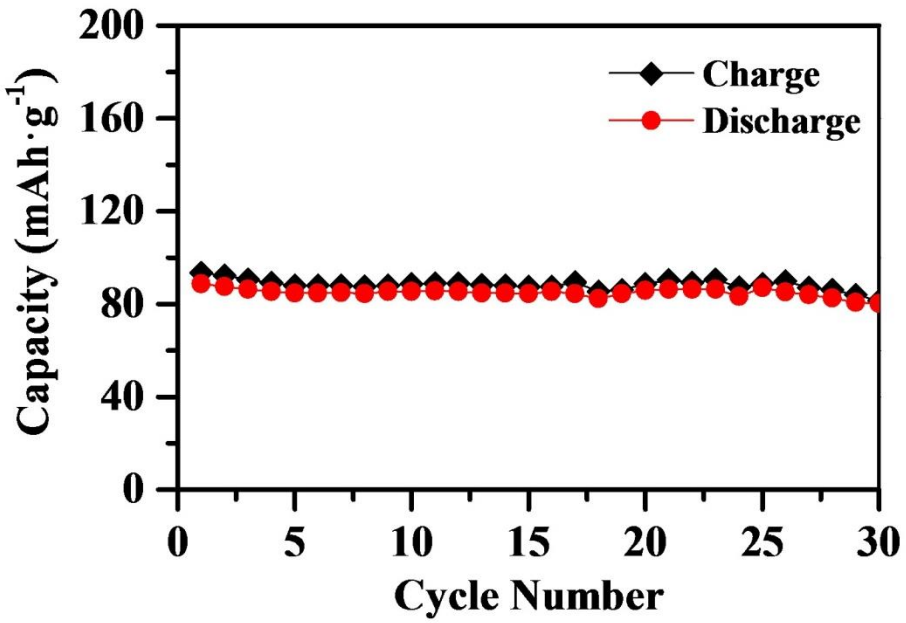

Fig.S18 Cycling performance of the sodium ion full battery at 50 mA g^{-1} (the specific capacity is calculated based on anode materials)

References

[S1] Wang, W.; Yu, C.; Lin, Z.; Hou, J.; Zhu, H.; Jiao, S.; *Nanoscale* **2013,** *5(2)*, 594.

[S2] Rudola, A.; Saravanan, K.; Mason, C.; Balaya, P.; *J. Mater.Chem. A* **2013,** *1(7)*, 2653.

[S3] Pan, H.; Lu, X.; Yu, X.; Hu, Y.; Li, H.; Yang, X.; Chen, L.; *Adv. Energy Mater.* **20**13, *3(9)*, 1186.

[S4] Zhang, Y.; Guo, L.; Yang, S. *Chem. Commun.* **2014,** *50*, 14029.

[S5] Shaju, K.; SubbaRao, G.; Chowdari, B.; *Electrochimi.Acta* **2003,** *48 (18)*, 2691.

[S6] Yan, Z.; Liu, L.; Shu, H.; Yang, X.; Wang, H.; Tan, J.; Zhou, Q.; Huang, Z.; Wang, X.; *J. Power Sources* **2013,** *244*, 758;

[S7] Deng, C.; Zhang, S.; Dong, Z.; Shang, Y.; *Nano Energy* **2014,** *4*, 49.

[S8] Zhang, Y.; Xie, J.; Zhu, T.; Cao, G.; Zhao, X.; Zhang, S.; *J. Power Sources* **2014,** *247*, 204.

[S9] Abel, P.; Lin, Y.; Souza, T. de; Chou, C.; Gupta A.; Goodenough J.; Hwang G.; Heller, A.; Mullins, C.; *J. Phys. Chem. C* **2013,** *117 (37)*, 18885.